

How low can the fractional quantum Hall effect go?

Zheng-Wei Zuo^{1,2,†}, Ajit C. Balram^{3,†}, Songyang Pu¹, Jianyun Zhao¹, A. Wójs,⁴ and J. K. Jain¹

¹*Department of Physics, The Pennsylvania State University, University Park, Pennsylvania 16802, USA*

²*School of Physics and Engineering, and Henan Key Laboratory of Photoelectric Energy Storage Materials and Applications, Henan University of Science and Technology, Luoyang 471023, China*

³*The Institute of Mathematical Sciences, HBNI, CIT Campus, Chennai 600113, India and*

⁴*Department of Theoretical Physics, Wrocław University of Science and Technology, 50-370 Wrocław, Poland*

(Dated: June 12, 2022)

While it is generally believed that a crystal state is favored at filling factors $\nu < 1/6$ in the lowest Landau level, experiments show, at elevated temperatures, minima in the longitudinal resistance that are associated with fractional quantum Hall effect (FQHE) at the standard sequences $\nu = n/(6n \pm 1)$ and $\nu = n/(8n \pm 1)$. To address this paradox, we investigate the nature of the state at filling factors $\nu = 1/7, 1/9, 1/11$ and $2/13$ by several methods and find that the competition between the crystal and liquid states is more subtle than previously thought. Exact diagonalization study in the spherical geometry shows behavior consistent with an FQHE liquid for system sizes available. Density matrix renormalization group study in the cylindrical geometry shows that the nature of the state depends on the particle number, with crystal favored for certain particle numbers but not all; these studies do not allow us to make conclusive statements regarding the thermodynamic nature of the state. A variational study shows that the composite-fermion crystal and the renormalized FQHE liquid are very close in energy. Based on these studies, it is not possible to rule out, definitively, an FQHE liquid with strong short-range crystalline correlations at these filling factors.

PACS numbers: 73.43.-f, 71.10.Pm

I. INTRODUCTION

The physics of the fractional quantum Hall effect (FQHE), right from its beginning^{1,2}, has been intertwined with the physics of the expected Wigner crystal phase in the lowest Landau level (LLL)^{3,4}. There has been a great deal of theoretical^{5–13} and experimental^{14–36} work addressing this issue, and the following picture is widely believed: (i) At filling factors $\nu = n/(2n \pm 1)$, $\nu = n/(4n \pm 1)$, where n is a positive integer, and their hole partners, the ground state is a FQH liquid. These states are understood as integer quantum Hall (IQH) state of composite fermions (CFs)³⁷, which are bound states of electrons and an even number of quantized vortices. (ii) In n-doped GaAs quantum wells, an insulating phase is seen between $\nu = 1/5$ and $\nu = 2/9$ and also below $\nu = 1/5$ ^{16,17}. A strong case may be made that these insulators represent a crystal pinned by the disorder. Similarly, insulating states, seen in the vicinity of $\nu = 1/3$ ^{20,21} are also viewed as disorder-pinned crystals. (iii) Theoretically, it has been demonstrated that the crystal of composite fermions^{11–13} is energetically better than the crystal of electrons. The number of vortices bound to composite fermions is fewer than the maximum number of available vortices, which leaves composite fermions with enough freedom to form a crystal. (For example, at $1/7$ and $1/9$, the best crystals have 4 and 6 vortices bound to composite fermions.) In particular, the crystal formed in between $1/5$ and $2/9$ is explained as a crystal of ²CFs, namely composite fermions carrying two quantized vortices¹². (iv) Finally, the FQHE terminates for $\nu < 1/5$, where the crystal phase dominates.

It is the last assertion (iv) that we address in this article. The motivation is as follows. Experiments clearly

show that the state for $\nu < 1/5$ is insulating with exponentially high resistance at the lowest temperatures. At the same time, signatures of FQHE at $\nu = 1/7$ and $2/11$ have been reported by Goldman *et al.*³⁸ and Mallett *et al.*³⁹, respectively. Moreover, Pan *et al.*²⁴ observe developing FQH states at $\nu = 2/11, 3/17, 3/19, 2/13, 1/7, 2/15, 2/17$, and $1/9$ at elevated temperatures, which belong to the standard Jain ⁶CF and ⁸CF sequences at $\nu = n/(6n \pm 1)$ and $\nu = n/(8n \pm 1)$.

There are two possible explanations for these observations.

Scenario I: In the absence of disorder, the ground state at filling factors of the type $\nu = n/(6n \pm 1)$ and $\nu = n/(8n \pm 1)$ is an incompressible FQH liquid, but slightly away from these filling factors the crystal prevails (analogously to what happens near $\nu = 1/5$). As a result, the filling factor variation due to disorder creates domains of crystal, and sufficiently large filling factor variation prevents percolation of the FQH liquid, producing an exponentially large resistance at low temperatures. Nonetheless, the presence of FQH domains produces resistance minima at the special filling factors. This scenario is depicted in Fig. 1, and is consistent with the known experimental facts.

Scenario II: The ground state in the absence of disorder is a crystal, which is pinned by the disorder to produce insulating behavior. As the temperature is raised, the crystal melts into a correlated FQH liquid. In this scenario, the composite fermions in the crystal phase will bind additional vortices when the crystal melts to produce the observed behavior. While in principle possible, this would be somewhat counter-intuitive, because one expects composite fermions to lose their vortices as the temperature is raised.

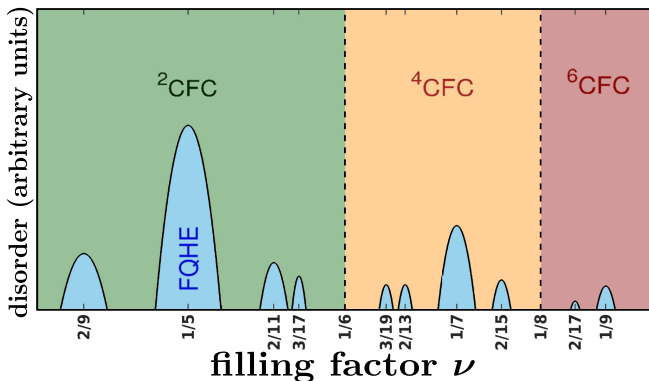


FIG. 1. Schematic phase diagram implied by the Scenario I (see text). The acronyms ${}^2\text{CFC}$, ${}^4\text{CFC}$ and ${}^6\text{CFC}$, refer respectively to crystals of composite fermions carrying two, four and six vortices.

A definitive experiment to distinguish between the two scenarios would be to determine whether the resistance minima at the special filling factors appear only above certain “melting” temperature (a pure crystal phase cannot have any FQHE-like signatures) or whether they persist to arbitrarily low temperatures. The difficulty is that at low temperatures the resistance becomes too large to measure. In the published experiments^{24,38,39}, however, the minima are seen whenever the resistance is measurable; in fact, the minima do not disappear with lowering the temperature but rather deepen relative to the exponentially rising background.

For these reasons, we revisit the belief that the region below $\nu < 1/5$ is dominated by the crystal phase. The issue is ultimately an energetic one and requires an accurate understanding of both the liquid and the crystal phases. We find that the competition between the FQHE liquid and the crystal phases is much more subtle than previously believed. Based on our current calculations we are not able to rule out that, in an ideal situation, FQHE is stabilized at fractions of the form $\nu = n/(6n \pm 1)$ and $\nu = n/(8n \pm 1)$. Our studies indicate that if the FQHE liquid were to be stabilized at these fractions, it will have strong short-range crystalline correlations.

We provide here a summary obtained from three different methods we apply to this problem. Throughout this work, we shall assume that the external magnetic field is strong enough to fully spin polarize the electrons. Furthermore, we shall consider an ideal system with zero width, zero LL mixing, and no disorder.

Exact diagonalization (ED): We perform exact diagonalization (ED) studies in the spherical geometry, going to much larger systems than before. In our studies, we find that the states at $\nu = 1/7$, $2/13$, $1/11$, and $1/9$ appear to be incompressible FQH liquid states by all measures. They have uniform ground states, i.e. have total orbital angular momentum $L = 0$ in the spherical geometry, which is an important property of incompressible

states (for other states, in general, $L > 0$). They have the expected excitation spectrum and have robust charge and neutral gaps that extrapolate to non-zero values in the thermodynamic limit. The ground states have a large overlap with the Laughlin or Jain wave functions. For $N = 10$ particles, the exact energy as a function of flux also shows downward cusps at the special filling factors $\nu = 1/7$ and $2/13$. If we were to base our conclusion solely on these studies, there would be no reason to suspect a crystal phase. We note that there are two possible problems with our ED studies: i) The systems accessible to us are finite, and there is no guarantee that the behavior will not change for larger systems. ii) The spherical geometry disfavors a crystal because a triangular crystal cannot be perfectly accommodated on the surface of a sphere. Nonetheless, Scenario II would suggest a ground state with a non-zero L .

Density matrix renormalization group (DMRG): Earlier calculations in the torus⁹ and disk¹¹ geometries favored a crystal phase at $\nu = 1/7$ and $\nu = 1/9$; these calculations were performed for $N = 6$ and thus not necessarily indicative of the behavior in the thermodynamic limit. It was shown in Ref.⁴⁰ that the crystal state wins over the liquid even for $\nu = 1/5$ for small systems, and it is necessary to go to sufficiently large systems (with $N \geq 10$) to see that the actual state is an FQHE liquid. To see if analogous physics might be present at $\nu = 1/7$ and $\nu = 1/9$, we have performed extensive DMRG studies in the cylindrical geometry. We find that for certain particle numbers, such as $N = 6$ and $N = 12$ the crystal appears to be favored, but for other values of N (e.g. $N = 9, 16$) the situation is less clear. We also find that while a liquid state is unambiguous for $\nu = 1/3$, the behavior seen in theoretical calculations at $\nu = 1/7$ is not qualitatively different from that at $\nu = 1/5$. Based on the particle numbers available to us, we are not able to make a conclusive statement regarding the nature of the state at $\nu = 1/7$ and $1/9$ in the thermodynamic limit. Our calculations do indicate that even if the actual ground state is a liquid, it has strong short-range crystalline correlations.

Variational Monte Carlo (VMC): The exact diagonalization and DMRG studies are restricted to finite systems. We have therefore also performed variational Monte Carlo studies. The validity of the variational studies depends on the accuracy of the wave functions used in the study. For the crystal phase, the CF crystal wave functions are extremely accurate at low filling factors¹¹. We find that the CF crystal has lower energy than the “bare” Laughlin/Jain wave functions^{2,37} for $\nu = 1/7$, $2/13$ and $1/9$. (The ${}^4\text{CF}$ crystal has the lowest energy at $\nu = 1/7$, and the ${}^6\text{CF}$ crystal has the lowest energy at $\nu = 1/9$) However, the bare Laughlin/Jain wave functions are not very accurate representations of the liquid at small fillings^{11,41}. The variational energy of the liquid state can be significantly improved by allowing a renormalization of composite fermions through dressing by CF excitons, using the method of CF diagonalization⁴². We

find that after such renormalization, the energies of the CF liquids become competitive with those of the CF crystals in the thermodynamic limit.

The plan for the rest of the paper is as follows. We first provide a primer on composite fermion theory and spherical geometry in Sec. II. In Section III A we provide results obtained from our extensive exact diagonalization studies on the sphere. Results obtained from variational Monte Carlo calculations on the sphere using the CF wave functions are given in Sec. III C. Section IV contains results from DMRG calculations. The paper is concluded in Section V with a brief discussion of our results and a summary of our conclusions.

II. PRIMER ON SPHERICAL GEOMETRY AND COMPOSITE FERMION THEORY

Our exact diagonalization and variational Monte Carlo calculations are carried out on the Haldane sphere⁴³, where N electrons are confined to the surface of a sphere in the presence of a radial magnetic flux of $2Qh/e$ ($2Q$ is an integer) generated by a magnetic monopole placed at the center of the sphere. Appropriate to this geometry, the total orbital angular momentum L and its z -component L_z are good quantum numbers. Incompressible quantum Hall states at filling factor ν occur on the sphere when $2Q = N/\nu - \mathcal{S}$, where \mathcal{S} is a topological quantum number called the shift⁴⁴. These states are distinguished by the fact that (i) they are uniform, i.e. have $L = 0$, for all N , and (ii) they have a non-zero gap to excitations in the thermodynamic limit. These are the criteria that we will use to ascertain whether the actual state is incompressible. In contrast, a compressible state, in general, has $L \neq 0$ and no well-defined gap.

The phenomenology of FQHE occurring in the LLL is understood using the CF theory^{37,45}, which maps strongly interacting electrons at filling factor $\nu = \nu^*/(2p\nu^* + 1)$ into weakly interacting CFs carrying $2p$ vortices at filling factor ν^* . One of the consequences of this mapping is that when $\nu^* = n$, where n is a positive integer, an incompressible FQH state of electrons occurs at filling factor $\nu = n/(2pn + 1)$. The Jain CF wave function for the incompressible FQH ground state at $\nu = n/(2pn + 1)$ is given by

$$\Psi_{n/(2pn+1)}^{\text{CF}} = \mathcal{P}_{\text{LLL}} \Phi_n \Phi_1^{2p}, \quad (1)$$

where Φ_n is the integer quantum Hall (IQH) state constructed at the effective magnetic monopole strength $2Q^* = N/n - n$. The symbol \mathcal{P}_{LLL} represents projection into the LLL, for which we use the Jain-Kamilla (JK) method^{45–50}. Because the shifts add, the incompressible state at $\nu = n/(2pn + 1)$ is predicted to occur at shift $\mathcal{S} = n + 2p$. The above wave function reduces to the Laughlin wave function for $\nu = 1/(2p + 1)$. The wave function of the ground state as well as the excitations obtained from the CF theory accurately capture the corresponding true Coulomb states in the LLL^{45,46,48,51–57}.

Similarly, using the analogy to the IQH effect, wave functions for the low-energy excitations of the FQH state, namely quasiparticles and quasiholes (which are created upon removal or insertion of flux quanta in the ground state) can also be constructed. In particular, CF theory predicts that the total orbital angular momentum of the single quasihole (QH) or single quasiparticle (QP) state at $\nu = n/(2pn + 1)$ is $L^{\text{QH}} = (N + (n - 1)^2)/(2n)$ and $L^{\text{QP}} = (N + n^2 - 1)/(2n)$. In particular, the single quasihole or single quasiparticle state at $\nu = 1/(2p + 1)$ is obtained respectively by the addition or removal of a single flux quantum h/e in the ground state and occurs at $L^{\text{QH}} = N/2 = L^{\text{QP}}$.

The Laughlin state at $\nu = 1/(2p + 1)^2$ is the unique densest exact zero-energy ground state of the short-range interaction specified by the two-body Haldane pseudopotentials $V_m = 1 \ \forall m \leq 2p$ and $V_m = 0 \ \forall m \geq 2p + 1$ ⁴³. Here V_m is the energy of a pair of electrons in the relative angular momentum state m . No local interactions in the LLL are known which produce the wave functions of Eq. (1) at other fractions as exact zero-energy ground states⁵⁸.

Next we describe the various electron and composite fermion crystal states considered in this work. Crystal states can occur when the electrons or composite fermions prefer to occupy localized wave packets to minimize the strong repulsion of the Coulomb interaction. In the spherical geometry, a wave packet localized at spinor coordinates (U, V) is created by $(uU^* + vV^*)^{2Q}$, where (u, v) are particle coordinates. The $2p$ -vortex composite fermion crystal (2^pCFC) wave function is given by

$$\Psi_{2Q}^{2^p\text{CFC}} = \prod_{i < j} (u_i v_j - u_j v_i)^{2p} \text{Det} \left[(u_i U_j^* + v_i V_j^*)^{2Q^*} \right]. \quad (2)$$

Here $2Q^* = 2Q - 2p(N - 1)$ and only those values of p are allowed that lead to a positive value of $2Q^*$. The $p = 0$ case corresponds to the electron crystal. We choose the crystal sites to lie at the Thomson locations^{59–62}, which minimizes the classical Coulomb repulsion energy of point particles on a sphere. Note that a triangular crystal, which is what the electrons organize themselves into in two dimensions to minimize the Coulomb repulsion energy, in the spherical geometry necessarily has some defects. However, we shall obtain the crystal energies by extrapolation of energies of very large systems and take the thermodynamic limit where the correction due to defects vanishes.

III. RESULTS FROM CALCULATIONS ON SPHERICAL GEOMETRY

In this section we discuss all the results obtained in the spherical geometry. These include results obtained from exact diagonalization (Sec. III A), entanglement spectra (Sec. III B) and variational Monte Carlo (Sec. III C).

A. Exact diagonalization

We have performed calculations for larger systems than before, going to $N = 10$ for $\nu = 1/7$, $N = 9$ for $\nu = 1/9$ and $1/11$. These systems correspond to Hilbert space dimensions of 1.1×10^9 , 0.6×10^9 , and 3.4×10^9 , respectively (to calculate the charged gaps we needed to go one flux quantum above the ground states, making the size of the diagonalized matrices even slightly larger).

The key innovation used to efficiently diagonalize such large matrices is that in the on-the-fly matrix-times-vector multiplication done at each Lanczos iteration we exploit the following symmetry of the two-body interaction: states with the same $N - 2$ occupied orbitals and different only by the pair of states occupied by the last two electrons form a sequence distinguished by a single two-body scattering. Importantly, a two-body scattering connects any two states of this sequence. Hence, there is a nonzero matrix element for each element of the corresponding submatrix, and it is equal to the corresponding two-body scattering amplitude. Since the most time-consuming part of the matrix-times-vector product is finding the location (row and column) of a given amplitude in the matrix, filling the matrix by consecutive submatrices is a relatively fast approach. On the downside, efficient parallelization with this method requires more memory than in approaches which divide the matrix into disconnected rows. For the systems with dimensions exceeding 10^9 such computation with 24-fold parallelization requires at least 512GB of RAM (widely accessible today) and yields speeds of one Lanczos iteration per a couple of hours (real-time) and a total time of a couple of weeks to typically reach convergence for the ground state.

We find that the exact Coulomb ground states at $1/7$, $1/9$, $1/11$ and $2/13$ have $L = 0$ for all N studied. This is significant because a ground state with $L \neq 0$ would indicate a compressible state (e.g. a crystal). The energies of finite size systems and their overlaps with the model Laughlin or Jain states are quoted in Table I. The exact Coulomb ground states have significant overlap with the Laughlin or Jain wave functions at these special fillings. In Fig. 2 we compare the pair-correlation function $g(r)$ of the exact LLL Coulomb ground state with that of the Laughlin state. We find that the $g(r)$ for these two states are in reasonable agreement with each other. Possibly there are crystalline correlations at short distances, with the strength of these correlations being much stronger in the exact LLL Coulomb ground state as compared to the Laughlin state. As $r \rightarrow 0$, for the $\nu = 1/(2p+1)$ Laughlin state, $g(r) \sim r^{2(2p+1)}$ while for the exact LLL Coulomb ground state $g(r) \sim r^2$ at all filling factors considered in this work.

The extrapolation of the exact LLL Coulomb ground state energies at fillings $\nu = 1/3$, $1/5$, $1/7$ and $1/9$ are shown in Fig. 3. These correlation energies include contributions of the electron-background and background-background interactions. We multiply the per-particle

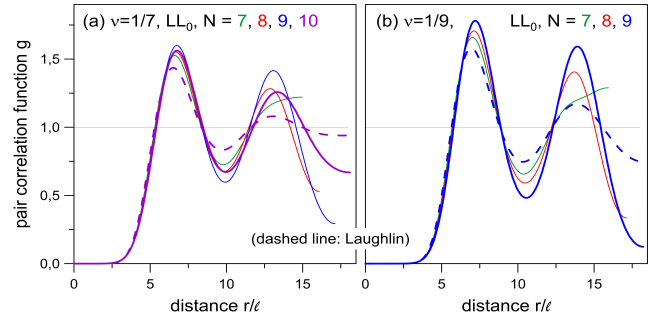


FIG. 2. (color online) Pair-correlation function $g(r)$ for the exact lowest Landau level Coulomb ground state (thick line) and Laughlin state (dashed line) at $\nu = 1/7$ (left panel) and $1/9$ (right panel).

energies by a factor of $\sqrt{2Q\nu/N}$ before extrapolating to $N \rightarrow \infty$ ⁶³. This factor corrects for the finite size deviation of the electron density from its thermodynamic value, thus providing a more accurate extrapolation.

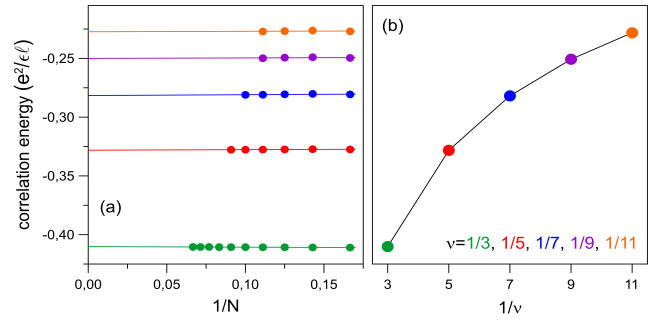


FIG. 3. (color online) Thermodynamic extrapolation of the exact lowest Landau level Coulomb ground state energies for fillings $\nu = 1/3$, $1/5$, $1/7$, $1/9$ and $1/11$. Left panel (a) shows the extrapolation obtained from energies of finite size systems in the spherical geometry and the right panel (b) shows the thermodynamic energies as a function of $1/\nu$. The correlation energies include interaction with the positively charged background and have been density corrected. All energies are quoted in units of $e^2/(\epsilon\ell)$.

An important characteristic of an incompressible state is that it costs finite energy to create charged excitations. Fig. 4 depicts the charge gap as a function of $1/N$ at fractions of the type $1/(2p+1)$. The charge gap at these Laughlin fractions is defined as the sum of the energies of a quasihole (QH) and a quasiparticle (QP), which in turn are determined from exact diagonalization at $2Q = (2p+1)(N-1) \pm 1$, respectively. We find that the total orbital angular momentum quantum number of the exact ground state at $2Q = (2p+1)(N-1) \pm 1$ is consistent with that predicted by the CF theory for all the systems considered in this work. The charge gap is equal to the energy required to create a far separated pair of quasihole and quasiparticle. From the extrapolation, we

can obtain the charge gap in the thermodynamic limit. While there are some finite-size fluctuations, at least from the system sizes available to us, the charge gaps appear to extrapolate to non-zero values for both $\nu = 1/7$ and $\nu = 1/9$. The extrapolated thermodynamic values of the charge gap are shown in Fig. 5 for several Laughlin fractions.

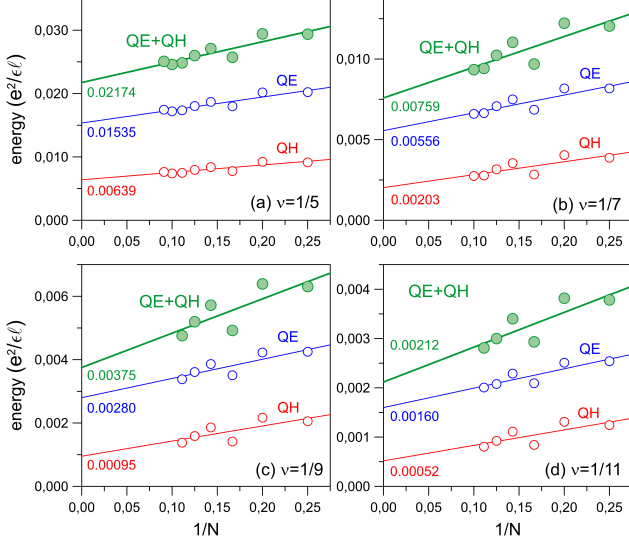


FIG. 4. (color online) The energy of the quasihole (QH), quasiparticle (QP), and their sum for the lowest Landau level Coulomb state at Laughlin fillings as a function of $1/N$, where N is the number of electrons. All the energies quoted in units of $e^2/(\epsilon\ell)$.

Next, we turn to neutral excitations at filling factors $1/(2p+1)$. The CF theory predicts that the lowest-energy neutral excitations are excitons of composite fermions, consisting of a single CF-particle-hole excitation. (The neutral exciton mode has also been called the magnetoroton mode.) The CF theory predicts that the exciton branch extends from angular momentum $L = 2$ to $L = N$. Our exact diagonalization study shows a clearly identifiable low-energy neutral mode extending from $L = 2$ to $L = N$. The dispersions of the magnetorotons at $1/7$ and $1/9$ are shown in Fig. 6. Due to strong finite-size effects, we have not been able to obtain a reliable thermodynamic extrapolation of the smallest neutral gap at low fillings.

Considering all these results we conclude that exact diagonalization studies on small systems are fully consistent with the formation of incompressible FQHE states at $\nu = 1/7$ and $\nu = 1/9$.

B. Entanglement spectra

We have also studied the edge excitations of the exact ground state by evaluating its entanglement spectrum. The entanglement spectrum has been useful in

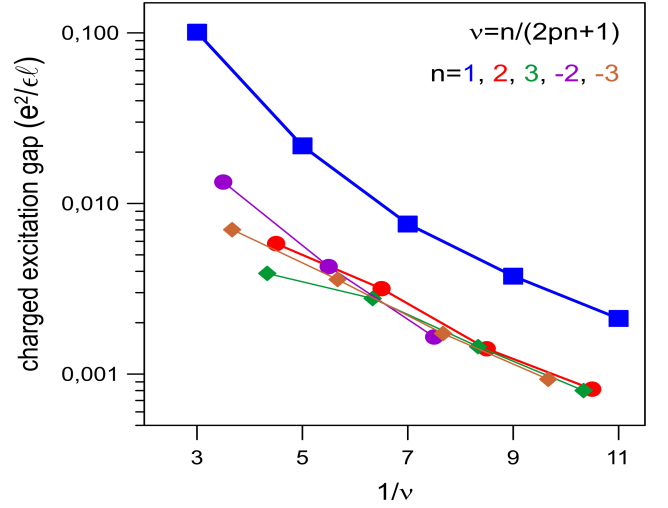


FIG. 5. (color online) Exact lowest Landau level Coulomb charge gap, which is the energy required to create a far-separated quasiparticle-quasihole pair, for fillings $\nu = n/(2pn + 1)$. The extrapolated gaps were obtained from a linear fit in $1/N$ of gaps of finite size systems in the spherical geometry (see Fig. 4 for extrapolations of the charge gap for Laughlin fillings). All energies are quoted in units of $e^2/(\epsilon\ell)$.

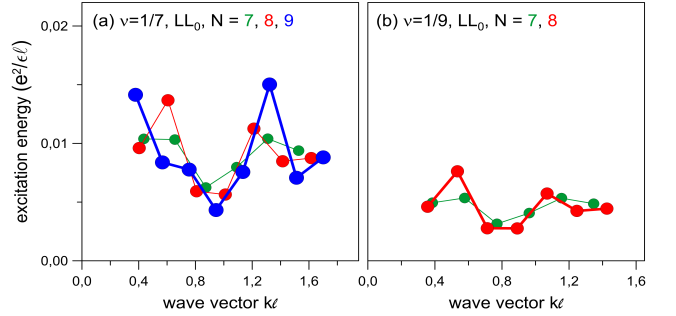


FIG. 6. (color online) Magnetoroton dispersions of the exact lowest Landau level Coulomb state at $1/7$ (left panel) and $1/9$ (right panel) as a function of the dimensionless wave vector $k\ell = L\ell/R$, where L is the total orbital angular and R is the radius of the sphere. All the energies quoted in units of $e^2/(\epsilon\ell)$ and are measured relative to the ground state energy.

characterizing many FQH states because the counting of low-lying entanglement levels characterizes the topological order of the state⁶⁴. To evaluate it from the ground state wave function $|\Psi\rangle$, we divide the system into two sub-systems A and B , so that the state can be written as: $|\Psi\rangle = \sum_{i,j} c_{ij} |\Psi_i^A\rangle \otimes |\Psi_j^B\rangle$ where $|\Psi_i^A\rangle$ and $|\Psi_j^B\rangle$ are the basis states for the A and B sub-systems respectively and c_{ij} are the expansion coefficients. We then do a Schmidt decomposition to obtain: $|\Psi\rangle = \sum_k e^{-\xi_k/2} |\Psi_k^A\rangle \otimes |\Psi_k^B\rangle$, where ξ_k are the entanglement eigenvalues which form the entanglement spectrum. Fig. 7 shows the orbital entanglement spectrum⁶⁵ of the

ν	N	$2Q$	$\dim_{L_z=0}$	$\dim_{L=0}$	exact	liquid energies ($e^2/(\epsilon\ell)$)		crystal energies ($e^2/(\epsilon\ell)$)				overlap
						bare	renormalized	electron crystal	CF crystal			
						Laughlin/Jain	up to 3 CF excitons		^2CF	^4CF	^6CF	$ \langle\psi^{\text{exact}} \psi^{\text{L/J}}\rangle $
1/7	4	21	241	4	-0.279799	-0.279320(0)	-0.27980(0)	-0.27366(5)	-0.27671(8)	-0.27814(5)	-	0.9741
	5	28	2,649	7	-0.279223	-0.279157(0)	-0.27920(1)	-0.27198(7)	-0.27546(8)	-0.27729(7)	-	0.9972
	6	35	32,134	47	-0.280706	-0.279773(0)	-0.28069(0)	-0.27576(0)	-0.27852(6)	-0.27966(3)	-	0.8716
	7	42	413,442	229	-0.280217	-0.279841(0)	-0.28021(0)	-0.27370(9)	-0.27701(4)	-0.27857(4)	-	0.9631
	8	49	5,557,206	1,985	-0.280580	-0.279987(0)	-0.28055(0)	-0.27498(0)	-0.27792(2)	-0.27927(7)	-	0.9097
	9	56	77,182,439	17,487	-0.280911	-0.280117(0)	-0.28086(1)	-0.27573(6)	-0.27853(3)	-0.27973(1)	-	0.8348
	10	63	1,099,923,868	178,665	-0.28104	-0.280204(0)	-0.28098(2)	-0.27593(3)	-0.27868(0)	-0.27985(8)	-	0.8119
1/9	4	27	519	5	-0.248519	-0.248141(0)	-0.248516(0)	-0.24448(8)	-0.24613(3)	-0.24703(5)	-0.24768(0)	0.9736
	5	36	7,483	10	-0.247875	-0.247832(0)	-0.247872(0)	-0.24312(7)	-0.24498(0)	-0.24616(3)	-0.24690(0)	0.9970
	6	45	118,765	91	-0.249628	-0.248674(0)	-0.249595(0)	-0.24654(5)	-0.247916(6)	-0.248663(3)	-0.24908(7)	0.8277
	7	54	1,999,265	624	-0.248967	-0.248666(0)	-0.248950(0)	-0.24481(6)	-0.24647(7)	-0.24758(6)	-0.24821(8)	0.9583
	8	63	35,154,340	7,105	-0.249424	-0.248855(0)	-0.249381(0)	-0.24598(5)	-0.24746(2)	-0.24832(1)	-0.24872(5)	0.8789
	9	72	638,724,335	84,470	-0.249817	-0.249018(0)	-0.249752(1)	-	-	-	-	0.7762
2/13	4	18	150	3	-0.288781	-0.288751(0)	-0.288751(1)	-0.28119(6)	-0.28530(6)	-0.28722(0)	-	0.9992
	6	31	17,002	34	-0.289873	-0.289540(0)	-0.289853(1)	-0.28394(6)	-0.28748(6)	-0.28881(9)	-0.28892(7)	0.9642
	8	44	2,502,617	1,137	-0.289885	-0.289723(0)	-0.289751(1)	-0.28344(3)	-0.28702(9)	-0.28852(9)	-0.28896(5)	0.9820
	10	57	421,777,505	85,250	-0.290440	-0.290063(0)	-0.290321(1)	-0.28449(3)	-0.28792(8)	-0.28922(3)	-0.28928(9)	

TABLE I. Background-subtracted density-corrected per-particle lowest Landau level (LLL) Coulomb energies for various liquid and crystal states at filling factors $\nu = 1/7, 1/9$ and $2/13$. The last column shows the absolute value of the overlap of the exact state with the trial Laughlin(L)/Jain(J) state^{2,37}. The number in the parenthesis is the statistical uncertainty of the Monte Carlo calculation of the energies.

exact LLL Coulomb ground state at $\nu = 1/7$ for a system of $N = 8$ electrons at a flux of $2Q = 49$ on the sphere. The counting of the low-lying entanglement levels of the exact LLL Coulomb ground state $\nu = 1/7$ is identical to that of the Laughlin state which indicates that the two states lie in the same topological phase.

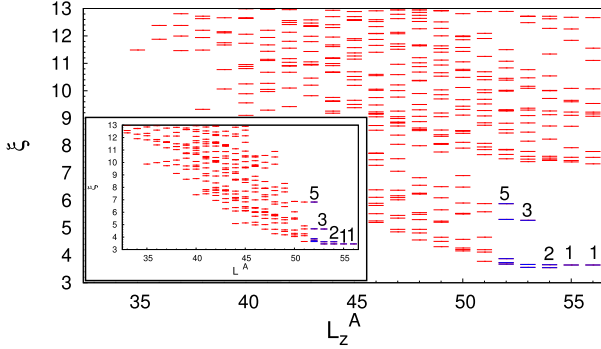


FIG. 7. (color online) Orbital entanglement spectrum at $\nu = 1/7$ of the exact lowest Landau level Coulomb ground state and the Laughlin state (inset) for $N = 8$ electrons at a flux $2Q = 49$ on the sphere. The two subsystems A and B with respect to which the entanglement spectrum is calculated have $N_A = N_B = 4$ electrons and $L_A = L_B = 25$ orbitals. The entanglement levels are labeled by the z -component of the total orbital angular momentum of the subsystem A , L_z^A . The counting of low-lying levels (from $L_z^A = 56$ and going from right to left) goes as 1, 1, 2, 3, 5, ..., which matches with the $U(1)$ chiral boson counting.

C. Variational Monte Carlo studies

Using the wave functions given in Eq. (1) we calculate the Coulomb energy of the FQHE liquid states at $\nu = 1/7, 2/13$ and $1/9$ for large systems using the Metropolis Monte Carlo method⁶⁶. As with the exact diagonalization results, to obtain the thermodynamic limit of the per-particle energy we first multiply the energy of finite systems by a factor of $\sqrt{2Q\nu/N}$ before extrapolating to $N \rightarrow \infty$ ⁶³. The “bare” Laughlin/Jain wave functions of Eq. (1) do not give the best description of the liquid ground state at the low fillings considered in our work⁴¹. The variational estimate of the liquid energies can be significantly improved by dressing the bare state with CF excitons. The energy of this renormalized ground state is calculated by the method of composite fermion diagonalization (CFD)^{42,45}. We quote energies of the liquid state at $\nu = 1/7, 2/13$ and $1/9$ obtained by renormalizing the Laughlin/Jain state by dressing it with up to three CF excitons. In Table I we show results for small systems where we compare the liquid energies against exact diagonalization. From the table, we see that the dressed liquid energies are very close to the exact energies. A thermodynamic extrapolation of the bare and dressed liquid energies is shown in Fig. 8.

We also evaluate the Coulomb energies of various crystal states of Eq. (2) using the Monte Carlo method. A thermodynamic extrapolation of the energies of the electron and CF crystal states is shown in the Fig. 8 and the estimated thermodynamic values are given in Table II. At $\nu = 1/7$ and $2/13$, the ${}^4\text{CF}$ crystal has the lowest energy, whereas at $\nu = 1/9$ the ${}^6\text{CF}$ crystal has the lowest energy.

Fig. 9 shows a plot of Coulomb ground state energy in the LLL for $N = 10$ electrons as a function of the flux $2Q$. The downward cusps in the correlation energies obtained

ν	exact energies ($e^2/(\epsilon\ell)$)	liquid energies ($e^2/(\epsilon\ell)$)		crystal energies ($e^2/(\epsilon\ell)$)			
		bare	renormalized	electron crystal	CF crystal		
		Laughlin/Jain	3 CF excitons		${}^2\text{CF}$	${}^4\text{CF}$	${}^6\text{CF}$
1/7	-0.2819(5)	-0.28094(1)	-0.2820(3)	-0.2788(9)	-0.2810(3)	-0.2820(3)	same as Laughlin
1/9	-0.2508(8)	-0.24997(1)	-0.2510(5)	-0.2493(8)	-0.2506(7)	-0.2514(0)	-0.2514(4)
2/13	-	-0.29087(1) ⁵⁰	-0.2912(1)	-0.2880(8)	-0.2907(9)	-0.2914(9)	-

TABLE II. Thermodynamic limit of the lowest Landau level (LLL) Coulomb ground state energies of the liquid and crystal states at filling factors $\nu = 1/7, 1/9$ and $2/13$. For comparison we also show the numbers obtained from exact diagonalization studies. All energies are quoted in units of $e^2/(\epsilon\ell)$. The number in the parenthesis denotes the uncertainty in the linear extrapolation of the energies as a function of $1/N$, where N is the number of electrons.

from exact diagonalization at $\nu = 1/7$ and $\nu = 2/13$ suggest that the states here are incompressible. On the other hand, we find that the energies of the best crystal vary smoothly with $2Q$.

The primary conclusion from variational comparisons is the following. In the thermodynamic limit the energies of the CF crystal and the dressed liquid are consistent, within numerical uncertainty, with one another, and also with the energies obtained from exact diagonalization studies, at the fractions studied (see Table II). The competition between the liquid and the CF crystal states at low fillings is thus rather subtle.

IV. DMRG STUDIES

A. DMRG method

Since the development of the density matrix renormalization group (DMRG) algorithm^{67,68} and its description in terms of matrix product state (MPS) representation⁶⁹, this algorithm has become a reliable approach to precisely calculate ground states and their energies for one-dimensional quantum many-body systems. Through mapping the two-dimensional electrons under a strong magnetic field in the lowest Landau level to a one-dimensional lattice model, DMRG algorithms have been used to investigate the FQHE liquids and composite fermion Fermi sea⁷⁰⁻⁷⁴. Here we apply the DMRG approach to the cylindrical geometry using the Landau gauge, following Zaletel, Mong and Pollmann⁷².

The cylindrical geometry is topologically equivalent to a parallelogram in the complex plane, which has periodic boundary condition in one direction and open boundary condition in the other. The two edges of parallelogram are L and $L\tau$, where the complex number $\tau = \tau_1 + i\tau_2$ is known as the modular parameter. The particle coordinate is given by $z = x + iy = L(\theta_1 + \tau\theta_2)$, where $\theta_1, \theta_2 \in [-0.5, 0.5)$. The real axis is chosen to be the periodic direction of cylinder with a circumference of L . The axis of the cylinder is along $L\tau$ with open boundary condition. Using the Landau gauge $A = (-y, 0)/\ell^2$, we can obtain the single particle wave-function in LLL⁷²:

$$\varphi_n(\theta_1, \theta_2) = (2\tau_2 N_{\text{orb}})^{1/4} e^{i2\pi n(\theta_1 + \theta_2\tau_1)} e^{-\pi\tau_2 N_{\text{orb}} \left(\theta_2 - \frac{n}{N_{\text{orb}}}\right)^2} \quad (3)$$

where N_{orb} is the number of orbits and index n takes values $0, 1, \dots, N_{\text{orb}} - 1$. The wave function $\varphi_n(\theta_1, \theta_2)$ satisfies the periodic boundary condition $\varphi_n(\theta_1 + 1, \theta_2) = \varphi_n(\theta_1, \theta_2)$, which can be viewed as a one-dimensional lattice model with lattice constant 1. For a finite size system with N particles at filling $\nu = 1/m$, the number of orbitals $N_{\text{orb}} = m(N - 1) + 1$ which is the same as that on the spherical geometry⁷⁵.

As noted in Ref.⁷⁶, the long range nature of the Coulomb interaction leads to divergences on a cylinder. To avoid this divergence, we choose the interaction $V(\mathbf{r}) = \frac{e^{-\mu r}}{r}$, which reduces to the Coulomb interaction for $\mu = 0$. The total energy is composed of four terms:

$$E_{\text{total}} = E_{ee} + E_{eb} + E_{bb} + E_{\text{self}} \quad (4)$$

The last two terms on the right-hand side, which represent the background-background interaction and self-interaction due to periodic geometry, are just constant numbers and can be omitted in the calculation of density profiles and pair-correlation functions. The energies are quoted in units of $e^2/(\epsilon\ell)$. The first two terms represent the electron-electron interaction and electron-background interaction. The corresponding Hamiltonians in second quantized form are given by:

$$H_{ee} = \sum_{n,k \geq |m|}^{N_{\text{orb}}} V_{mk}^{ee} c_{n+m}^\dagger c_{n+k}^\dagger c_{n+m+k} c_n \quad (5)$$

$$V_{mk}^{ee} = 2(V_{mk} - V_{km}) \quad (6)$$

$$V_{mk} = \frac{e^{-\frac{\pi\tau_2 m^2}{N_{\text{orb}}}}}{L\tau_2} \int_0^\infty dq_2 \frac{e^{-\left[\frac{(q_2 - 2\pi m\tau_1)^2}{4\pi\tau_2 N_{\text{orb}}}\right]} \cos\left(\frac{(q_2 - 2\pi m\tau_1)k}{N_{\text{orb}}}\right)}{\sqrt{(2\pi m)^2 + \left(\frac{q_2 - 2\pi m\tau_1}{\tau_2}\right)^2 + \mu^2 L^2}} \quad (7)$$

$$H_{eb} = \sum_n V_n^{eb} c_n^\dagger c_n \quad (8)$$

$$V_n^{eb} = -\frac{2N}{L\tau_2 N_{\text{orb}}} \int_0^\infty dq_2 \frac{\cos\left(\frac{q_2(j-n)}{N_{\text{orb}}}\right) e^{-\frac{q_2^2}{4\pi\tau_2 N_{\text{orb}}}}}{\sqrt{q_2^2/\tau_2^2 + \mu^2 L^2}}, \quad (9)$$

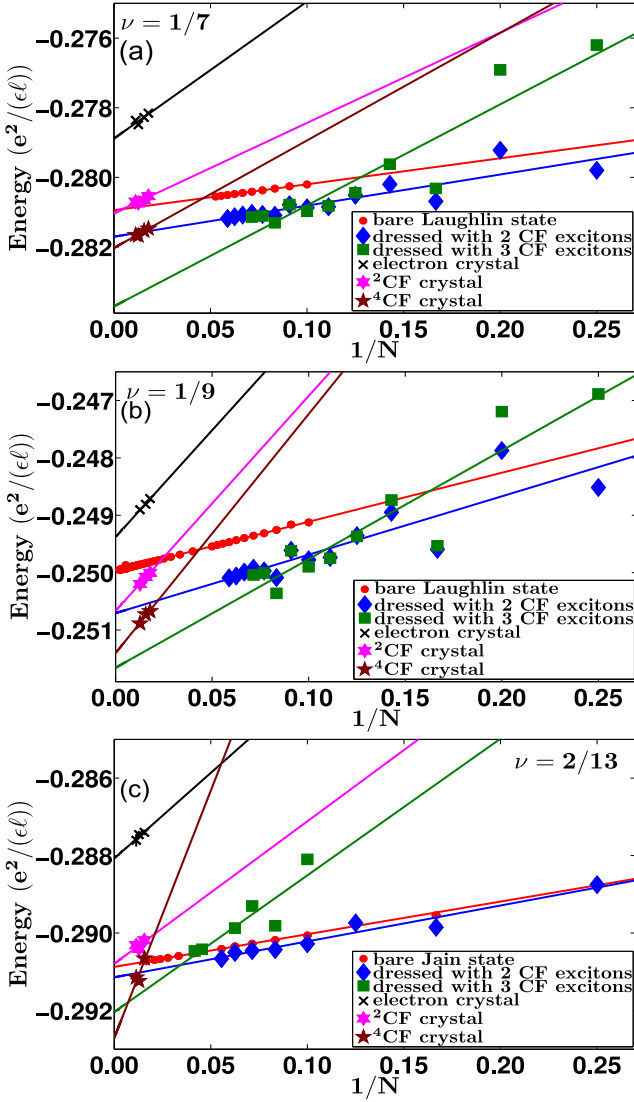


FIG. 8. (color online) Thermodynamic extrapolation of the lowest Landau level Coulomb ground state energies of the CF liquid and crystal states at filling factors $\nu = 1/7$ (top panel), $\nu = 1/9$ (center panel) and $\nu = 2/13$ (bottom panel). The error bars on the individual data points indicate the statistical Monte Carlo uncertainty in the energies. The energies of the $2/13$ bare Jain state and $2/13$ state dressed with two composite fermion (CF) excitons have been reproduced from Ref.⁵⁰. The extrapolated energies are tabulated in Table II.

where c_n^\dagger and c_n are the creation and annihilation operators for single particle orbital φ_n . Here the background charge distribution is chosen to be proportional to the electron charge distribution of lowest filled Landau level, i.e. $\rho_b(\mathbf{r}) = \frac{N}{N_{\text{orb}}} \sum_{n=1}^{N_{\text{orb}}} |\varphi_n(\mathbf{r})|^2$.

We use the pair correlation function to distinguish between the Wigner crystal and the FQH liquid states. The pair correlation function for our finite size system is de-

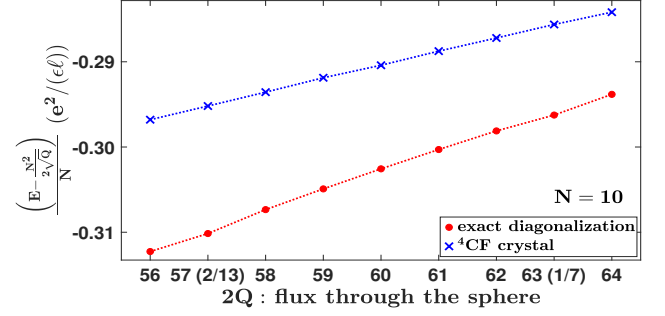


FIG. 9. (color online) A plot of the lowest Landau level Coulomb energies for $N = 10$ electrons as a function of the flux $2Q$ on the sphere. Cusps in the ground state energies can be seen at the special filling factors $\nu = 1/7$ and $2/13$ in the exact diagonalization data. This should be contrasted from the energies of the best crystal (that formed from composite fermions carrying four vortices), which is a smooth function of the filling factor. The dotted lines are just a guide to the eye.

fined as

$$g(\mathbf{r}, \mathbf{r}') = \frac{A}{\rho N} \left\langle \sum_{i \neq j} \delta(\mathbf{r} - \mathbf{r}_i) \delta(\mathbf{r}' - \mathbf{r}_j) \right\rangle \quad (10)$$

where $A = L^2 \tau_2$ is the area of the system. The DMRG algorithm is based on the ITensor library⁷⁷.

B. DMRG results

In Fig. 10, we show the occupation number and electron density profiles at the $\nu = 1/3$ filling for a $N = 24$ system with $\tau_1 = 0, \tau_2 = 1, \mu = 0.01$. We also show the pair correlation function by placing an electron in the center of square. For this DMRG calculation, the maximum bond dimension is $\chi = 33400$. To remove the effect of nonuniform density profile $\rho(\mathbf{r})$ on pair correlation function $g(\mathbf{r})$, in Fig. 10(d) we shown the normalized pair correlation function $g'(\mathbf{r}) = \frac{Ng(\mathbf{r})}{A\rho(\mathbf{r})}$. One can clearly see from the normalized pair correlation function that it is a FQH liquid at $\nu = 1/3$. We also note that there is no significant change in $g'(\mathbf{r})$ if we further lower the value of μ . The state at $1/3$ is unquestionably a liquid. This is also confirmed in our results shown below.

We next come to lower filling factors $1/5, 1/7$ and $1/9$. For finite systems, the cylindrical geometry also complicates the analysis of the crystal state. To properly capture the crystal, we choose a hexagonal cylinder with $\tau = 1/2 + i\sqrt{3}/2$ to match the triangular lattice. Even then, as shown in Fig. 11, the particle numbers which satisfy $N = n(n+1)$ (with n being an integer) are more “friendly” to crystal formation.

In Figs. 12, 13, and 14 we show results for systems with $N = 6, 9$ and 12 at $\nu = 1/3, 1/5, 1/7$ and $1/9$. Fig. 15

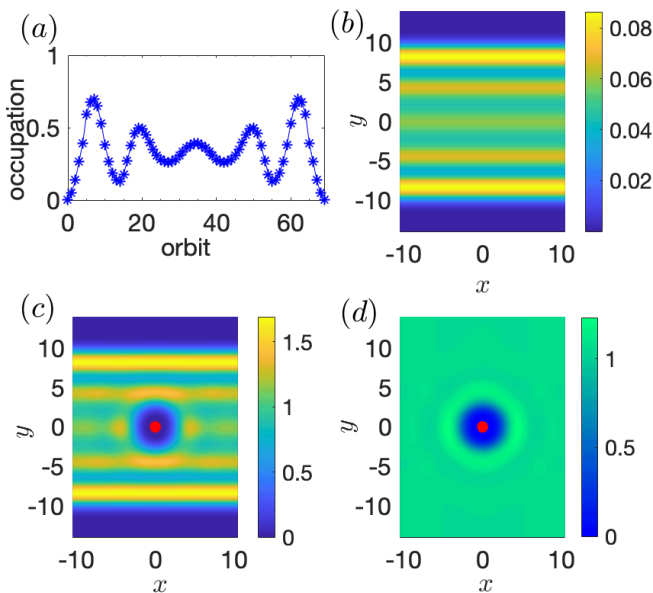


FIG. 10. The orbital occupation number, electron density profiles and pair correlation function for the $\nu = 1/3$ filling with the $N = 24$, $\tau_1 = 0$, $\tau_2 = 1$, $\mu = 0.01$. (a) Orbit occupation number (b) Electron density profiles $\rho(\mathbf{r})$. (c) Pair correlation function $g(\mathbf{r})$. (d) Normalized pair correlation function $g'(\mathbf{r})$. The red dots in (c-d) indicates one electron position we choose. Period boundary condition is applied to the horizontal direction and open boundary condition for vertical direction.

shows the pair correlation of 16 particles for $\nu = 1/7$. We choose $\mu = 0.0001$; we have found that our results are insensitive to the value of μ so long as $\mu \leq 0.01$. We show the density profiles (on the left) and pair correlation functions (on the right) for $N = 6, 9, 12$ in Fig. 12, Fig. 13, and Fig. 14, respectively. In the supplementary material⁷⁸, we show how the pair correlation function $g(\mathbf{r}, \mathbf{r}')$ changes as we vary the position of \mathbf{r} (indicated by a red dot in the figures) along the length of the cylinder.

The question, of course, is whether the system is a crystal or a liquid in the thermodynamic limit. The $\nu = 1/3$ state looks like a liquid for all particle numbers, so here there is no ambiguity. For $\nu = 1/5, 1/7$ and $1/9$, for 6 and 12 particles, the pair correlation function indicates a crystal phase, with the crystal centers becoming sharper as the filling factor is lowered. This indicates that crystalline correlations become stronger with decreasing ν . However, we are not able to conclusively rule out a liquid at $\nu = 1/7$ in the thermodynamic limit for two reasons. First, the behavior at $1/7$ closely resembles that at $1/5$, which is known to be a liquid. Second, for 9 and 16 particles, our results suggest a liquid phase at $\nu = 1/7$. We have not studied larger systems for $\nu = 1/9$ due to computational limitations.

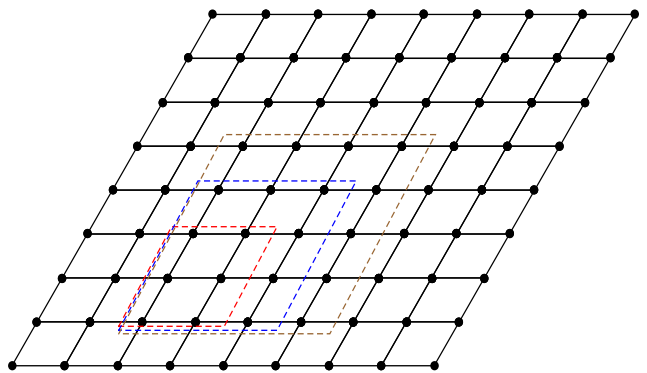


FIG. 11. Illustration of possible crystals formed on a finite cylinder with periodic boundary conditions in the x-direction. Because we have chosen a hexagonal cylinder, the two edges of the cylinder are of the same length. With that condition, and for periodic boundary conditions in the x-direction but with open boundaries in the y-direction, certain systems with $N = n(n+1)$ particles, where n is an integer, are more friendly to crystal formation. Specifically, the red, blue and brown dashed lines depict crystals with 6, 12 and 20 particles, respectively. Here we assume that electrons can be placed at the lower and the upper edges of the cylinder, which is not exactly obeyed in the real system; in reality, the hexagonal crystal is slightly squeezed in the y-direction due to the finite system effect of the open boundary. Nonetheless, this figure gives an idea of how finite cylinders make crystals more preferred for certain particle numbers.

V. CONCLUSION

In this article, we have revisited the issue of the nature of the state, i.e. whether it is an incompressible liquid or a crystal, at small filling factors, especially $\nu = 1/7$ and $\nu = 1/9$. We find that the issue is more subtle than previously thought. Exact diagonalization studies in the spherical geometry are fully consistent with an incompressible FQHE state here. On the other hand, DMRG studies in the cylindrical geometry are inconclusive. A variational study finds that the energies of the CF crystal and a renormalized FQH liquid are too close to call. We are thus not able to draw a definitive conclusion, except that if the state is an FQHE liquid, it has strong short-range crystalline correlations.

ACKNOWLEDGMENTS

The work at Penn State (S.P., J.Z., J.K.J.) was supported by the U. S. Department of Energy under Grant no. DE-SC0005042. Some portions of this research were conducted with Advanced CyberInfrastructure computational resources provided by The Institute for CyberScience at The Pennsylvania State University and the Nandadevi supercomputer, which is maintained and supported by the Institute of Mathemat-

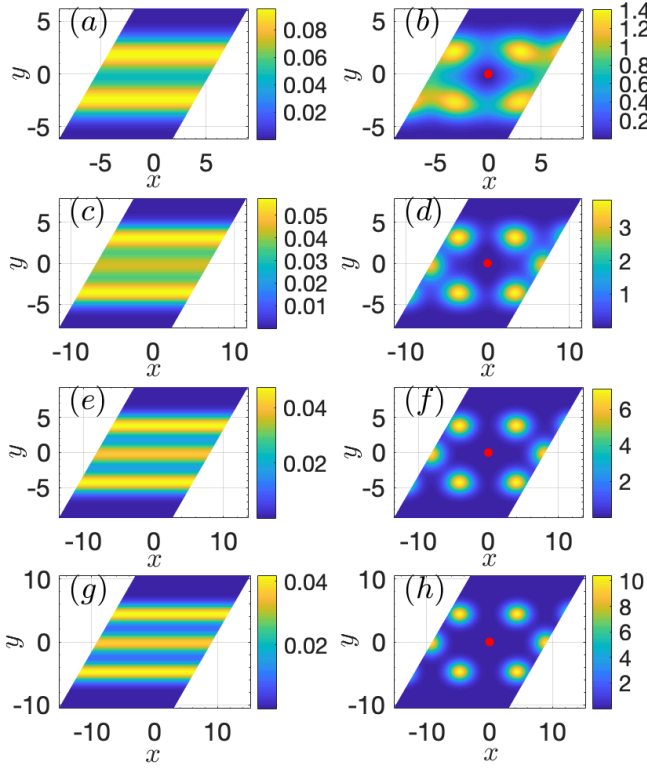


FIG. 12. The electron density (left panels) and pair correlation function (right panels) for $N = 6$ particles on a hexagonal cylinder. The results are for filling factors $\nu = 1/3$ (top row), $1/5$ (second row), $1/7$ (third row), and $1/9$ (bottom row). The red dots in the right panels (b, d, f, h) indicate the position of a fixed electron. We take periodic boundary condition for the horizontal direction and open boundary condition for the vertical direction.

cal Sciences High-Performance Computing Center. This work was also supported by the Polish NCN Grant No. 2014/14/A/ST3/00654 (A. W.). We thank Wrocław Centre for Networking and Supercomputing and Academic Computer Centre CYFRONET, both parts of PL-Grid Infrastructure. Some of the numerical calculations were performed using the DiagHam package, for which we are grateful to its authors. Z.W.Z. was also supported by the National Natural Science Foundation of China under grant numbers 11604081, 11447008. We thank the Tianhe-2 platform at the National Supercomputer Center in Guangzhou for technical support and a generous allocation of CPU time.

[†]Z. W. Z. and A. C. B. contributed equally to this work.

- ¹ D. C. Tsui, H. L. Stormer, and A. C. Gossard, Phys. Rev. Lett. **48**, 1559 (1982), URL <http://link.aps.org/doi/10.1103/PhysRevLett.48.1559>.
- ² R. B. Laughlin, Phys. Rev. Lett. **50**, 1395 (1983), URL <http://link.aps.org/doi/10.1103/PhysRevLett.50.1395>.
- ³ E. Wigner, Phys. Rev. **46**, 1002 (1934).
- ⁴ Y. E. Lozovik and V. I. Yudson, JETP Lett. **22**, 11 (1975).
- ⁵ K. Maki and X. Zotos, Phys. Rev. B **28**, 4349 (1983).
- ⁶ P. K. Lam and S. M. Girvin, Phys. Rev. B **30**, 473 (1984).
- ⁷ D. Levesque, J. J. Weis, and A. H. MacDonald, Phys. Rev. B **30**, 1056 (1984).
- ⁸ H. Yi and H. A. Fertig, Phys. Rev. B **58**, 4019 (1998).
- ⁹ K. Yang, F. D. M. Haldane, and E. H. Rezayi, Phys. Rev. B **64**, 081301 (2001).
- ¹⁰ R. Narevich, G. Murthy, and H. A. Fertig, Phys. Rev. B **64**, 245326 (2001).
- ¹¹ C.-C. Chang, G. S. Jeon, and J. K. Jain, Phys. Rev. Lett. **94**, 016809 (2005).
- ¹² A. C. Archer, K. Park, and J. K. Jain, Phys. Rev. Lett. **111**, 146804 (2013).
- ¹³ J. Zhao, Y. Zhang, and J. K. Jain, Phys. Rev. Lett. **121**, 116802 (2018), URL <https://link.aps.org/doi/10.1103/PhysRevLett.121.116802>.
- ¹⁴ M. Shayegan, in *Perspectives in Quantum Hall Effects* (Wiley-VCH Verlag GmbH, 2007), p. 343384, ISBN 9783527617258, URL <http://dx.doi.org/10.1002/9783527617258.ch10>.
- ¹⁵ H. A. Fertig, in *Perspectives in Quantum Hall Effects* (Wiley-VCH Verlag GmbH, 2007), p. 71108, ISBN 9783527617258, URL <http://dx.doi.org/10.1002/9783527617258.ch10>.
- ¹⁶ H. W. Jiang, R. L. Willett, H. L. Stormer, D. C. Tsui, L. N. Pfeiffer, and K. W. West, Phys. Rev. Lett. **65**, 633 (1990).
- ¹⁷ V. J. Goldman, M. Santos, M. Shayegan, and J. E. Cunningham, Phys. Rev. Lett. **65**, 2189 (1990).
- ¹⁸ F. I. B. Williams, P. A. Wright, R. G. Clark, E. Y. Andrei, G. Deville, D. C. Glatthi, O. Probst, B. Etienne, C. Dorin, C. T. Foxon, et al., Phys. Rev. Lett. **66**, 3285 (1991), URL <https://link.aps.org/doi/10.1103/PhysRevLett.66.3285>.
- ¹⁹ M. A. Paalanen, R. L. Willett, R. R. Ruel, P. B. Littlewood, K. W. West, and L. N. Pfeiffer, Phys. Rev. B **45**,

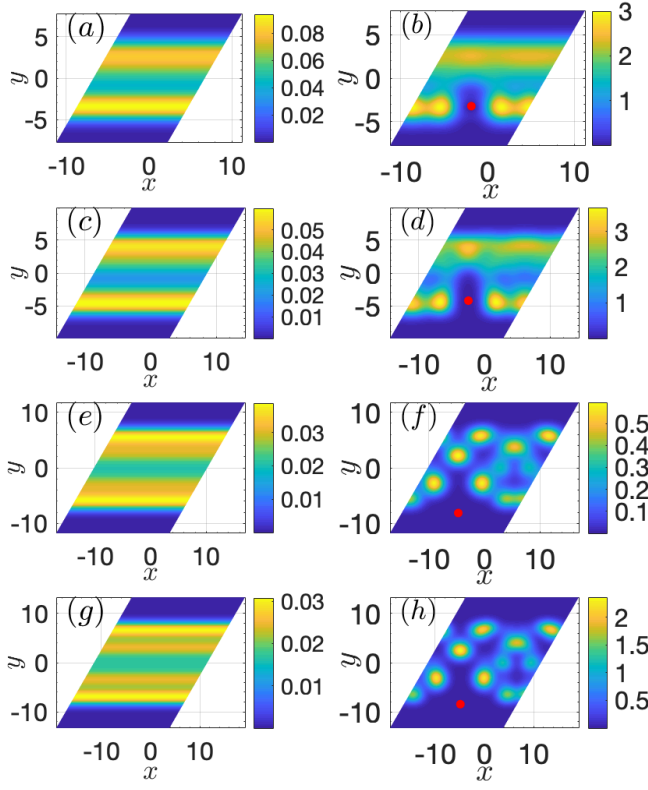


FIG. 13. Same as in Fig. 12 for $N = 9$ particles.

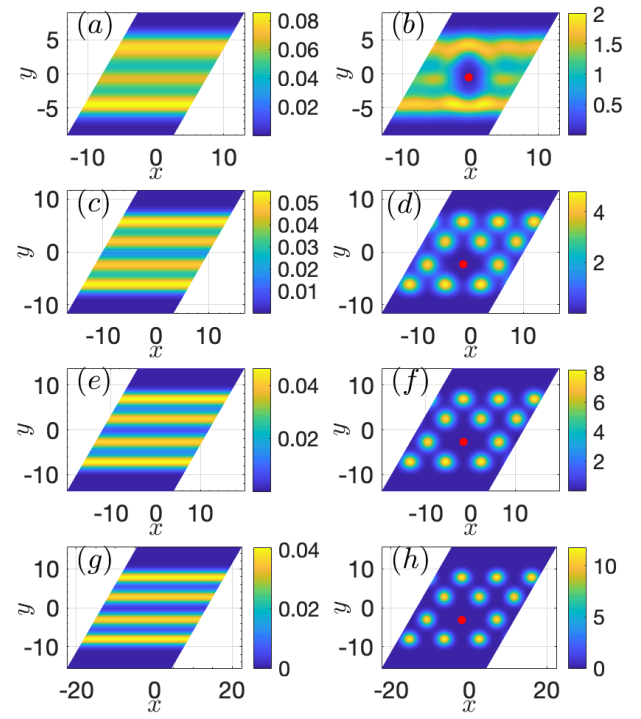


FIG. 14. Same as in Fig. 12 for $N = 12$ particles.

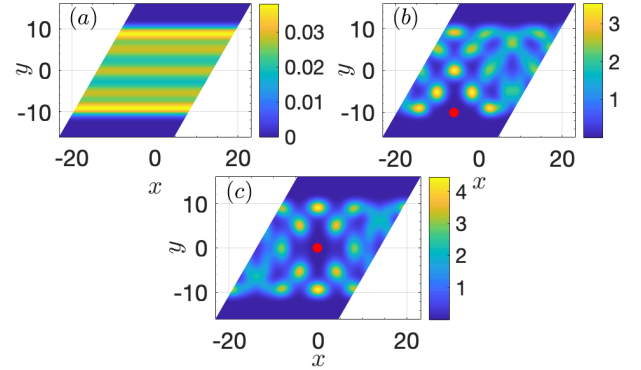


FIG. 15. The electron density (a) and pair correlation function at different positions (b,c) for the $\nu = 1/7$ for $N = 16$ particles. The other parameters are same as in Fig. 12.

13784 (1992), URL <http://link.aps.org/doi/10.1103/PhysRevB.45.13784>.

- ²⁰ M. B. Santos, Y. W. Suen, M. Shayegan, Y. P. Li, L. W. Engel, and D. C. Tsui, Phys. Rev. Lett. **68**, 1188 (1992).
- ²¹ M. B. Santos, J. Jo, Y. W. Suen, L. W. Engel, and M. Shayegan, Phys. Rev. B **46**, 13639 (1992), URL <https://link.aps.org/doi/10.1103/PhysRevB.46.13639>.
- ²² H. C. Manoharan and M. Shayegan, Phys. Rev. B **50**, 17662 (1994).
- ²³ L. Engel, C.-C. Li, D. Shahar, D. Tsui, and M. Shayegan, Physica E **1**, 111 (1997).
- ²⁴ W. Pan, H. L. Stormer, D. C. Tsui, L. N. Pfeiffer, K. W. Baldwin, and K. W. West, Phys. Rev. Lett. **88**, 176802 (2002).
- ²⁵ C.-C. Li, J. Yoon, L. W. Engel, D. Shahar, D. C. Tsui, and M. Shayegan, Phys. Rev. B **61**, 10905 (2000).
- ²⁶ P. D. Ye, L. W. Engel, D. C. Tsui, R. M. Lewis, L. N. Pfeiffer, and K. West, Phys. Rev. Lett. **89**, 176802 (2002).
- ²⁷ Y. P. Chen, R. M. Lewis, L. W. Engel, D. C. Tsui, P. D. Ye, Z. H. Wang, L. N. Pfeiffer, and K. W. West, Phys. Rev. Lett. **93**, 206805 (2004).
- ²⁸ G. A. Cs  thy, H. Noh, D. C. Tsui, L. N. Pfeiffer, and K. W. West, Phys. Rev. Lett. **94**, 226802 (2005).
- ²⁹ W. Pan, G. A. Cs  thy, D. C. Tsui, L. N. Pfeiffer, and K. W. West, Phys. Rev. B **71**, 035302 (2005), URL <https://link.aps.org/doi/10.1103/PhysRevB.71.035302>.
- ³⁰ G. Sambandamurthy, Z. Wang, R. Lewis, Y. P. Chen, L. Engel, D. Tsui, L. Pfeiffer, and K. West, Solid State Commun. **140**, 100 (2006).
- ³¹ Y. P. Chen, G. Sambandamurthy, Z. H. Wang, R. M. Lewis, L. W. Engel, D. C. Tsui, P. D. Ye, L. N. Pfeiffer,

and K. W. West, Nature Phys. **2**, 452 (2006).

- ³² Y. Liu, D. Kamburov, S. Hasdemir, M. Shayegan, L. N. Pfeiffer, K. W. West, and K. W. Baldwin, Phys. Rev. Lett. **113**, 246803 (2014), URL <http://link.aps.org/doi/10.1103/PhysRevLett.113.246803>.
- ³³ C. Zhang, R.-R. Du, M. J. Manfra, L. N. Pfeiffer, and K. W. West, Phys. Rev. B **92**, 075434 (2015), URL <https://link.aps.org/doi/10.1103/PhysRevB.92.075434>.
- ³⁴ H. Deng, Y. Liu, I. Jo, L. N. Pfeiffer, K. W. West, K. W. Baldwin, and M. Shayegan, Phys. Rev. Lett. **117**, 096601 (2016), URL <http://link.aps.org/doi/10.1103/PhysRevLett.117.096601>.
- ³⁵ J. Jang, B. M. Hunt, L. N. Pfeiffer, K. W. West, and R. C. Ashoori, Nature Physics **13**, 340 (2017), ISSN 1745-2473.

- ³⁶ S. Chen, R. Ribeiro-Palau, K. Yang, K. Watanabe, T. Taniguchi, J. Hone, M. O. Goerbig, and C. R. Dean, *Phys. Rev. Lett.* **122**, 026802 (2019), URL <https://link.aps.org/doi/10.1103/PhysRevLett.122.026802>.
- ³⁷ J. K. Jain, *Phys. Rev. Lett.* **63**, 199 (1989), URL <http://link.aps.org/doi/10.1103/PhysRevLett.63.199>.
- ³⁸ V. J. Goldman, M. Shayegan, and D. C. Tsui, *Phys. Rev. Lett.* **61**, 881 (1988).
- ³⁹ J. R. Mallett, R. G. Clark, R. J. Nicholas, R. Willett, J. J. Harris, and C. T. Foxon, *Phys. Rev. B* **38**, 2200 (1988), URL <https://link.aps.org/doi/10.1103/PhysRevB.38.2200>.
- ⁴⁰ C.-C. Chang, C. Töke, G. S. Jeon, and J. K. Jain, *Phys. Rev. B* **73**, 155323 (2006).
- ⁴¹ S. S. Mandal, M. R. Peterson, and J. K. Jain, *Phys. Rev. Lett.* **90**, 106403 (2003).
- ⁴² S. S. Mandal and J. K. Jain, *Phys. Rev. B* **66**, 155302 (2002), URL <https://link.aps.org/doi/10.1103/PhysRevB.66.155302>.
- ⁴³ F. D. M. Haldane, *Phys. Rev. Lett.* **51**, 605 (1983), URL <http://link.aps.org/doi/10.1103/PhysRevLett.51.605>.
- ⁴⁴ X. G. Wen and A. Zee, *Phys. Rev. Lett.* **69**, 953 (1992), URL <http://link.aps.org/doi/10.1103/PhysRevLett.69.953>.
- ⁴⁵ J. K. Jain, *Composite Fermions* (Cambridge University Press, New York, US, 2007).
- ⁴⁶ J. K. Jain and R. K. Kamilla, *Int. J. Mod. Phys. B* **11**, 2621 (1997).
- ⁴⁷ J. K. Jain and R. K. Kamilla, *Phys. Rev. B* **55**, R4895 (1997), URL <http://link.aps.org/doi/10.1103/PhysRevB.55.R4895>.
- ⁴⁸ G. Möller and S. H. Simon, *Phys. Rev. B* **72**, 045344 (2005), URL <http://link.aps.org/doi/10.1103/PhysRevB.72.045344>.
- ⁴⁹ S. C. Davenport and S. H. Simon, *Phys. Rev. B* **85**, 245303 (2012), URL <http://link.aps.org/doi/10.1103/PhysRevB.85.245303>.
- ⁵⁰ A. C. Balram, C. Töke, A. Wójs, and J. K. Jain, *Phys. Rev. B* **92**, 075410 (2015), URL <http://link.aps.org/doi/10.1103/PhysRevB.92.075410>.
- ⁵¹ G. Dev and J. K. Jain, *Phys. Rev. Lett.* **69**, 2843 (1992), URL <http://link.aps.org/doi/10.1103/PhysRevLett.69.2843>.
- ⁵² M. R. Peterson and J. K. Jain, *Phys. Rev. B* **68**, 195310 (2003), URL <http://link.aps.org/doi/10.1103/PhysRevB.68.195310>.
- ⁵³ D. Mujumder, S. Mandal, and J. Jain, *Nature Physics* **5**, 403 (2009).
- ⁵⁴ A. C. Balram, A. Wójs, and J. K. Jain, *Phys. Rev. B* **88**, 205312 (2013), URL <http://link.aps.org/doi/10.1103/PhysRevB.88.205312>.
- ⁵⁵ J. K. Jain, *Indian Journal of Physics* **88**, 915 (2014), ISSN 0974-9845, URL <http://dx.doi.org/10.1007/s12648-014-0491-9>.
- ⁵⁶ D. Majumder and S. S. Mandal, *Phys. Rev. B* **90**, 155310 (2014), URL <http://link.aps.org/doi/10.1103/PhysRevB.90.155310>.
- ⁵⁷ A. C. Balram and J. K. Jain, *Phys. Rev. B* **93**, 235152 (2016), URL <http://link.aps.org/doi/10.1103/PhysRevB.93.235152>.
- ⁵⁸ G. J. Sreejith, M. Fremling, G. S. Jeon, and J. K. Jain, *Phys. Rev. B* **98**, 235139 (2018), URL <https://link.aps.org/doi/10.1103/PhysRevB.98.235139>.
- ⁵⁹ J. J. Thomson, *Phil. Mag.* **7**, 237 (1904).
- ⁶⁰ The minimum energy locations can be found at <http://thomson.phy.syr.edu/>.
- ⁶¹ D. J. Wales and S. Ulker, *Phys. Rev. B* **74**, 212101 (2006), URL <https://link.aps.org/doi/10.1103/PhysRevB.74.212101>.
- ⁶² D. J. Wales, H. McKay, and E. L. Altschuler, *Phys. Rev. B* **79**, 224115 (2009), URL <https://link.aps.org/doi/10.1103/PhysRevB.79.224115>.
- ⁶³ R. Morf, N. d'Ambrumenil, and B. I. Halperin, *Phys. Rev. B* **34**, 3037 (1986), URL <http://link.aps.org/doi/10.1103/PhysRevB.34.3037>.
- ⁶⁴ H. Li and F. D. M. Haldane, *Phys. Rev. Lett.* **101**, 010504 (2008), URL <http://link.aps.org/doi/10.1103/PhysRevLett.101.010504>.
- ⁶⁵ M. Haque, O. Zozulya, and K. Schoutens, *Phys. Rev. Lett.* **98**, 060401 (2007), URL <https://link.aps.org/doi/10.1103/PhysRevLett.98.060401>.
- ⁶⁶ K. Binder and D. Heermann, *Monte Carlo Simulation in Statistical Physics* (Springer-Verlag Berlin Heidelberg, 2010).
- ⁶⁷ S. R. White, *Phys. Rev. Lett.* **69**, 2863 (1992), URL <https://link.aps.org/doi/10.1103/PhysRevLett.69.2863>.
- ⁶⁸ U. Schollwöck, *Rev. Mod. Phys.* **77**, 259 (2005), URL <https://link.aps.org/doi/10.1103/RevModPhys.77.259>.
- ⁶⁹ U. Schollwöck, *Ann. Phys.* **326**, 96 (2011), URL <http://www.sciencedirect.com/science/article/pii/S0003491610001752>.
- ⁷⁰ N. Shibata and D. Yoshioka, *Phys. Rev. Lett.* **86**, 5755 (2001), URL <https://link.aps.org/doi/10.1103/PhysRevLett.86.5755>.
- ⁷¹ A. E. Feiguin, E. Rezayi, C. Nayak, and S. Das Sarma, *Phys. Rev. Lett.* **100**, 166803 (2008), URL <https://link.aps.org/doi/10.1103/PhysRevLett.100.166803>.
- ⁷² M. P. Zaletel, R. S. K. Mong, and F. Pollmann, *Phys. Rev. Lett.* **110**, 236801 (2013), URL <https://link.aps.org/doi/10.1103/PhysRevLett.110.236801>.
- ⁷³ M. P. Zaletel, R. S. K. Mong, F. Pollmann, and E. H. Rezayi, *Phys. Rev. B* **91**, 045115 (2015), URL <http://link.aps.org/doi/10.1103/PhysRevB.91.045115>.
- ⁷⁴ S. D. Geraedts, M. P. Zaletel, R. S. K. Mong, M. A. Metlitski, A. Vishwanath, and O. I. Motrunich, *Science* **352**, 197 (2016), ISSN 0036-8075, <http://science.sciencemag.org/content/352/6282/197.full.pdf>, URL <http://science.sciencemag.org/content/352/6282/197>.
- ⁷⁵ G. Ortiz, Z. Nussinov, J. Dukelsky, and A. Seidel, *Phys. Rev. B* **88**, 165303 (2013), URL <https://link.aps.org/doi/10.1103/PhysRevB.88.165303>.
- ⁷⁶ S. Johri, Z. Papić, P. Schmitteckert, R. N. Bhatt, and F. D. M. Haldane, *New Journal of Physics* **18**, 025011 (2016), URL <http://stacks.iop.org/1367-2630/18/i=2/a=025011>.
- ⁷⁷ ITensor Library (Version 3), URL <http://itensor.org>.
- ⁷⁸ See <https://github.com/zuozw/DMRG-FQHE> for the Supplemental Material which includes details for the pair correlation functions of other electron positions for all fillings.